

Anomalous changing of geodesics in hairy black holes

Weyner Ccuairo⁽¹⁾, David Choque⁽²⁾ and Gustavo Valdivia-Mera⁽³⁾

⁽¹⁾*Universidad Nacional de San Antonio Abad del Cusco,
Av. La Cultura 733, Cusco, Perú.*

⁽²⁾*Pontificia Universidad Católica de Valparaíso, Instituto de Física,
Av. Brasil 2950, Valparaíso, Chile.*

⁽³⁾*East African Institute for Fundamental Research (ICTP-EAIFR),
University of Rwanda, Kigali, Rwanda.*

October 18, 2022

Abstract

We study the motion of test particles and the propagation of light around neutral hairy black holes under the influence of a self-interacting real scalar field minimally coupled to gravity. The goal of the present work is to show that the time-like and null-like geodesics have an anomalous behaviour for a special range of parameters in the dense hair region, defined as $\sqrt{\Omega(x_h)} \leq r \leq 2MG_N/c^2$.

Contents

1	Introduction	2
2	Geodesics of Schwarzschild black hole	2
3	Hairy Black hole solution	3
3.1	Evading the no hair theorem	5
4	Time-like geodesics	7
5	Hairy null geodesics	8
6	Hairy near horizon geodesics	13
6.1	Time-like near horizon geodesics	13
6.2	Null-like near horizon geodesics	14
7	Discussion	15
A	Schwarzschild solution	17
A.1	Time-like geodesic	17
A.2	Null geodesic	21
B	Near-horizon geometry of Schwarzschild black hole	21
B.1	Time-like geodesics	23
B.2	Null geodesic	23

1 Introduction

Hairy solutions are extensively constructed in the context of different theories, in some cases with minimal and non-minimal coupling with the Einstein-Hilbert theory [1, 2, 3, 4, 5, 6, 7, 8, 9, 10]. In addition, there are many exact and numerical solutions for higher curvature theories [3, 11, 12, 13, 14]. Another relevant topic is the thermodynamic of hairy black holes [14, 15, 16, 17, 18, 19] where there are an interesting window of parameters in which the asymptotically flat hairy black holes are stable [20]. In the present work, we focus on the minimal coupling with real scalar field. It was constructed in [21, 22, 23], and consists of a general hairy family of asymptotically AdS solutions. Surprisingly if we fix, at the level of theory, $\Lambda = 0$ we get an exact hairy black hole solution which is asymptotically flat. That hairy solutions was studied extensively in [21, 24], and it can be embedded in SUGRA theories [4, 25, 26]. The hairy solutions presented here can evade the no-hair theorem [27], and the stability of the present hairy black holes is ensured by the scalar potential and its extreme points. Clearly, if I have only a kinetic term of the (real) scalar field in the theory, would not possible to evade the no-hair theorem, but if we add a non-minimal coupling gauge field it can behave like a scalar potential and there will be a possibility to evade the no-hair theorem [28]. When we have complex scalar fields or another exotic fields, it is required another details [29, 30]. Our purpose in the present article is consider an exact solution of one scalar field coupled to a static black hole.

An important motivation is the study the posible anomalous geodesics in hairy black holes. This family of hairy black hole solutions has a horizon radius r_h which is completely different from Schwarzschild radius $2MG_N/c^2$. We will show a concrete realization previously founded in [31], indeed we can prove that $r_h \leq 2MG_N/c^2$, then exist a region $\mathcal{D} \equiv 2MG_N/c^2 - r_h$ called the dense-hair region. That region has an important effect on the geodesics due to the backreaction of scalar field, which causes a geodesic anomalous deflection. In the figures of the black hole horizon, we use grey color to show the Schwarzschild region and black, for the hairy black hole. So, the region between them is the dense hair region \mathcal{D} . This simple and novel property has an interesting effect on geodesic configurations, which is highly relevant because it allows us, in future works, to build models that can be tested by analysis of the black hole's shadows, e.g. the Event Horizon Telescope: *The Shadow of the supermassive Black Hole* [32] and *The Shadow and Mass of the Central Black Hole* [33].

The qualitative nature will be studied in [34], and here we construct numerically the time-like and null-like trajectories. We use the Runge-Kutta method of fourth-order (RK4), which means that there are four parameters to obtain. The numerical plots and calculations were made in Python 3.8 [35] with the following libraries, NumPy [36], SciPy [37], Matplotlib [38]. All the plots of hairy black holes have been made using the library *hairyBH* [39] and for Schwarzschild see [40].

The present work is organized in the following form: First, in section 2, we consider a brief description of geodesics of Schwarzschild black hole, and its respective details are in the appendix A. In section 3, we describe the theory and properties of the hairy solution, such as the horizon existence and the mass for each branch. In section 4 and 5, we construct the orbital equation and solve it numerically. In addition, we present the plots of the effective potential and its respective trajectories for each region. In section 6, we construct the near horizon geometry for hairy black holes and we solve the geodesics equations, we verify the interesting anomalous changing of the geodesics shown in the following figures: 7b and 11a. Finally, in section 7, we present the discussion and future directions.

2 Geodesics of Schwarzschild black hole

All the details of the present section can be found in appendix A.1. The purpose of the present section is to show the geodesics of the Schwarzschild black hole and compare it with the hairy case. It is interesting that the Schwarzschild horizon radius is bigger than the radius of the hairy solution, and it means that the scalar field (hair) allows the existence of more compact objects. The geodesics for hairy black holes are studied in section 2. First, we show the null (see Figure 1) and time-like (see Figure 2) geodesics for Schwarzschild, where we have used $M = 10^6 M_\odot$, $\tilde{\mathcal{J}}^2 = 5.82708 \times 10^{-13} \text{yr}^2$ and $r_h \approx 0.019708 \text{AU}$. The numerical construction of geodesics

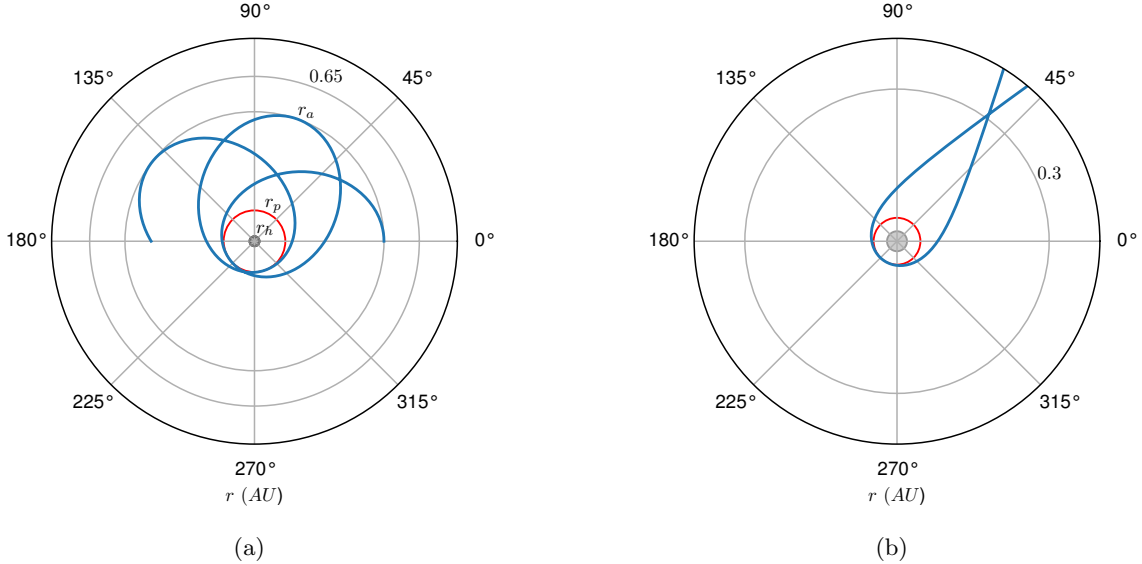


FIG. 1: **(Time-like)**

Here we consider: r_h (grey), r_p (red) and the orbit (blue). Where r_p indicates the radius of the minimum distance from the center of the black hole to the orbit.

(a): For energy $E = E_2 = -0.03$ and initial conditions: $r_0 = 0.51069 AU$ and $\dot{r}_0 = 0$. Where, $r_0 = r_a$ indicates the apoapsis, while $r_p = 0.12158 AU$, the periapsis. According to (A6) the angular deviation of the apoapsis per orbital period is $\Delta\varphi = 61.1^\circ$, you can verify that in this figure.

(b): $E = E_3 = 0.2$, initial conditions: $r_0 \rightarrow \infty$ and $\dot{r}_0 = \sqrt{E}c$. Where, $r_2 = 0.04613 AU$ indicates the radius of the minimum distance from the center of the black hole to the orbit.

is extensively know in the literature [11, 12, 13, 41].

In figure (2b) the geodesics fall into the black hole (Schwarzschild case), across the horizon, in a tangential form.

3 Hairy Black hole solution

We consider the following modified Einstein-Hilbert theory with an scalar field with non-minimal coupling

$$I[\mathbf{g}, \phi] = \frac{1}{2\kappa} \int_{\mathcal{M}} d^4x \sqrt{-g} R + \int_{\mathcal{M}} d^4x \sqrt{-g} \left[-\frac{1}{2} (\partial\phi)^2 - V(\phi) \right] \quad (1)$$

here the coupling constant is $\kappa = \frac{8\pi G_N}{c^4}$, where G_N is the constant of gravitation and c is the speed of light, g is the determinant of the metric tensor, $g = \det(g_{\mu\nu})$, R is the Ricci scalar and $V(\phi)$ is the self-interaction term. The equations of motion arising from the action principle are

$$G_{\mu\nu} = \kappa T_{\mu\nu}, \quad \frac{1}{\sqrt{-g}} \partial_\mu (\sqrt{-g} g^{\mu\nu} \partial_\nu \phi) = \frac{dV}{d\phi} \quad (2)$$

where the Einstein tensor and the energy-momentum tensor for the scalar field are respectively

$$\begin{aligned} G_{\mu\nu} &:= R_{\mu\nu} - \frac{1}{2} g_{\mu\nu} R \\ T_{\mu\nu} &= \partial_\mu \phi \partial_\nu \phi - g_{\mu\nu} \left[\frac{1}{2} (\partial\phi)^2 + V(\phi) \right] \end{aligned} \quad (3)$$

Following to [2, 16, 25, 42], we consider the exotic potential $V(\phi)$, it presents a non-trivially self-interaction, it was first obtained and presented in [25],

$$V(\phi) = \frac{\alpha}{\kappa\nu^2} \left\{ \frac{\nu-1}{\nu+2} \sinh[l_\nu(\nu+1)\phi] - \frac{\nu+1}{\nu-2} \sinh[l_\nu(\nu-1)\phi] + 4 \left(\frac{\nu^2-1}{\nu^2-4} \right) \sinh(l_\nu\phi) \right\} \quad (4)$$

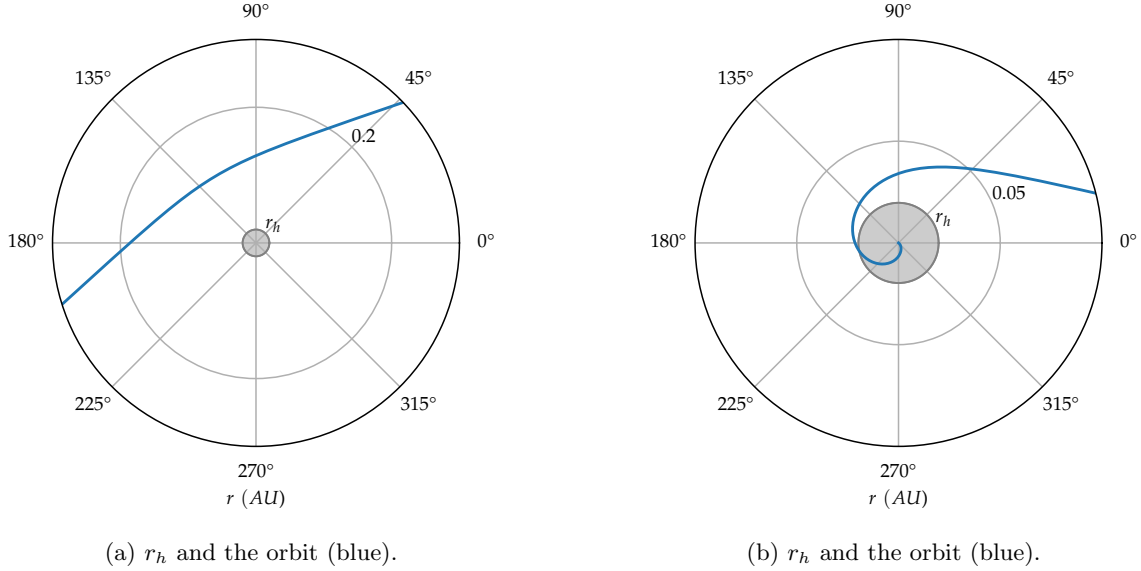


FIG. 2: (Null-like)

(a): $E = E_1 = 10^{21} AU^2 yr^{-4}$, initial conditions: $r_0 \rightarrow \infty$ and $\left(\frac{dr}{d\xi}\right)_0 = \sqrt{E}$. The impact parameter is given by $b^2 = 3.9993 \times 10^{-12} yr^2$. The light deviation can be calculated from (A10), we have $R_0 = 0.1188965650 AU$, them $|\Delta\varphi - \pi| \frac{180^\circ}{\pi} \approx 22^\circ$.

(b): $E = E_1 = 7.5 \times 10^{21} AU^2 yr^{-4}$, initial conditions: $r_0 \rightarrow \infty$ and $\left(\frac{dr}{d\xi}\right)_0 = \sqrt{E}$. The impact parameter is given by $b^2 = 5.3324 \times 10^{-13} yr^2$.

where $l_\nu \equiv \left(\frac{2\kappa}{\nu^2 - 1}\right)^{1/2}$. This theory has two novels parameters, α , which has an important role in the existence of the horizon and ν , which can calibrate the scalar field ϕ . Considering the following ansatz for conformal metric

$$ds^2 = \Omega(x) \left[-c^2 f(x) dt^2 + \frac{\eta^2 dx^2}{f(x)} + d\theta^2 + \sin^2 \theta d\varphi^2 \right] \quad (5)$$

we can integrate the equations of motion for the metric and scalar field, such that we obtain the family of hairy solutions [21, 22, 24, 43],

$$\phi(x) = l_\nu^{-1} \ln x \quad (6)$$

where the conformal factor $\Omega(x)$ and the metric function $f(x)$ are given by

$$\begin{aligned} \Omega(x) &= \frac{\nu^2 x^{\nu-1}}{\eta^2 (x^\nu - 1)^2} \\ f(x) &= \alpha \left[\frac{1}{\nu^2 - 4} - \frac{x^2}{\nu^2} \left(1 + \frac{x^{-\nu}}{\nu - 2} - \frac{x^\nu}{\nu + 2} \right) \right] + \frac{x}{\Omega(x)} \end{aligned} \quad (7)$$

Actually, there are two branches of spacetime in which the physical quantities are well defined. The quantity η is a positive definite constant of integration that is related to the mass of the black hole¹. The dimension of the parameter and constant of integration are $\dim \alpha = \dim \eta^2 = \text{length}^{-2}$ and $\dim \eta = \text{length}^{-1}$. In addition, ν is a dimensionless parameter.

¹Along the paper, we mostly use the unit system where the constants have the following values:

$$\begin{aligned} G_N &\approx 39.409 AU^3 M_\odot^{-1} yr^{-2}, \\ c &\approx 6.324 \cdot 10^4 AU yr^{-1}, \\ \kappa &\approx 6.192 \cdot 10^{-17} AU^{-1} M_\odot^{-1} yr^2 \end{aligned} \quad (8)$$

where M_\odot represents the solar mass, AU is for the Astronomical Unit and yr stands for a year

The principal characteristic of each branch are

- **Negative Branch:** The coordinate of the black hole horizon x_h is less than 1, then the range of the coordinate x is given by $x_h < x < 1$. The boundary is located at $x = 1$ and the singularity at $x = 0$. In this case the scalar field is negative definite $\phi < 0$
- **Positive Branch:** The coordinate of the black hole horizon x_h is greater than 1, then the range of the coordinate x is given by $1 < x < x_h$. The boundary is located at $x = 1$ and the singularity at $x = \infty$. Here the scalar field becomes positive definite $\phi > 0$

The radial coordinate system is more intuitive than conformal metric (5). The equation $r^2 = \Omega(x)$, which relates both coordinate systems, cannot be solved exactly but is easy to get the asymptotic coordinate transformation [44]

$$x = 1 \pm \frac{1}{\eta r} \mp \frac{\nu^2 - 1}{24\eta^3 r^3} \left[1 \mp \frac{1}{\eta r} \mp \frac{9(\nu^2 - 9)}{80\eta^2 r^2} \right] + \mathcal{O}(r^{-6}) \quad (9)$$

In [44, 45, 46, 47, 48, 49] you can find a quasilocal formalism used to find the mass (energy) of the gravitational system, and for asymptotically AdS spacetime in the presence of the scalar field [46]. The scalar field is a secondary hair, therefore, there is not a constant of integration associated to it, so, we have a unique constant of integration η which is just related with the mass. The ADM mass can be read-off from g_{tt} in canonical coordinates, in [34] we will construct a quasilocal stress tensor² (asymptotically flat) in order to get M , see [20, 52]

$$-\frac{1}{c^2} g_{tt} = 1 - \frac{2G_N M}{c^2 r} + \mathcal{O}(r^{-3}) \quad (10)$$

where the masses for negative branch and positive branch are respectively

$$M = \frac{c^2}{2G_N} \left(\frac{\alpha + 3\eta^2}{3\eta^3} \right), \quad \phi \leq 0 \quad (11)$$

$$M = -\frac{c^2}{2G_N} \left(\frac{\alpha + 3\eta^2}{3\eta^3} \right), \quad \phi \geq 0 \quad (12)$$

3.1 Evading the no hair theorem

The no hair theorem can be evaded if we have a potential with a global maximum at the boundary and a minimum at the horizon. That condition is ensured by $d^2V/d\phi^2 \leq 0$. Considering the following quantities for the spacetime $0 \leq x \leq 1$ which is named as negative branch $\phi \leq 0$:

- The potential $V(\phi)$ depends on the parameters ν and α . From figure (3), we check that $d^2V/d\phi^2 \leq 0 \Leftrightarrow \nu > 1, \alpha > 0$, and the scalar potential has a global minimum at the horizon $V(\phi_h)$.
- From figure (3), the horizon existence, $-\frac{g_{tt}}{c^2} = 0$, is ensured if $\alpha > 0$, and there is an additional condition for the mass:
 - For: $1 \leq \nu < 2$ there is no restriction on the mass of the black hole.
 - For: $2 < \nu$ in [2] they showed an interesting lower bound for the mass of hairy black holes which are asymptotically AdS, and here we present our result for asymptotically flat case. Clearly if the scalar field increase (that is dominated by hairy parameter ν) the black hole mass has a minimum value which can hold up the horizon

$$M > M_{cri} \equiv \frac{c^2}{2G_N} \left(\frac{\nu - 2}{\alpha} \right)^{1/2} \quad (13)$$

and for the spacetime $1 \leq x \leq \infty$ we have the positive branch $\phi \geq 0$:

- The potential $V(\phi)$ depends on the parameters ν and α . From figure (4b), we check that $d^2V/d\phi^2 \leq 0 \Leftrightarrow \nu > 1, \alpha < 0$ and the scalar potential has a global minimum at the horizon $V(\phi_h)$.

²For asymptotically AdS space-time here you can find an interesting discussions [50, 51]

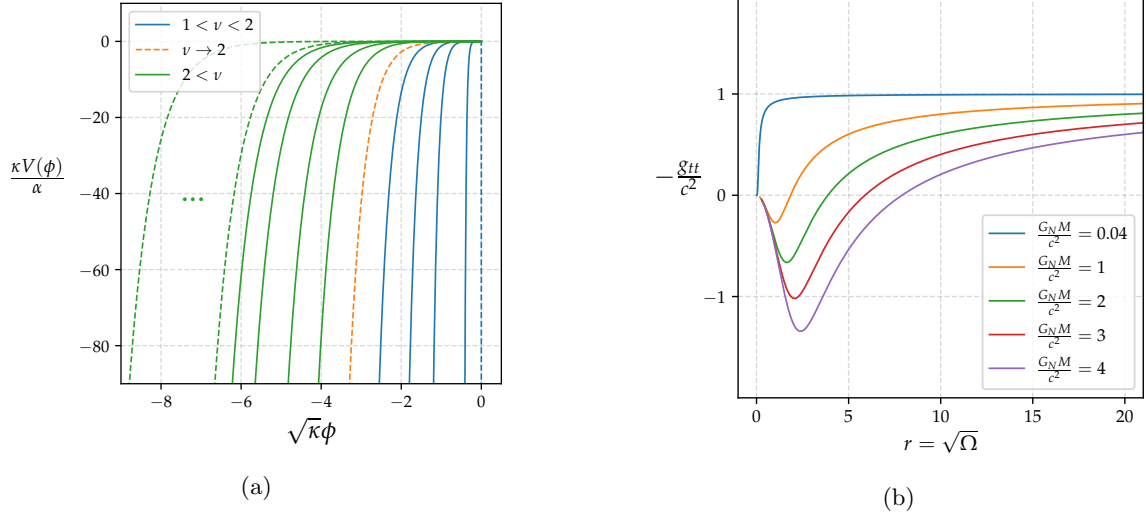


FIG. 3: Negative branch. (a): $\frac{\kappa}{\alpha}V(\phi)$ vs $\sqrt{\kappa}\phi$. (b): $-g_{tt}/c^2$ vs $\sqrt{\Omega}$: We consider the hairy parameter $\nu = 1.52$, $\alpha = 1 \text{ AU}^{-2}$ and the range of masses for the black holes $0.04 \text{ AU} \leq \frac{G_N M}{c^2} \leq 4.00 \text{ AU}$.

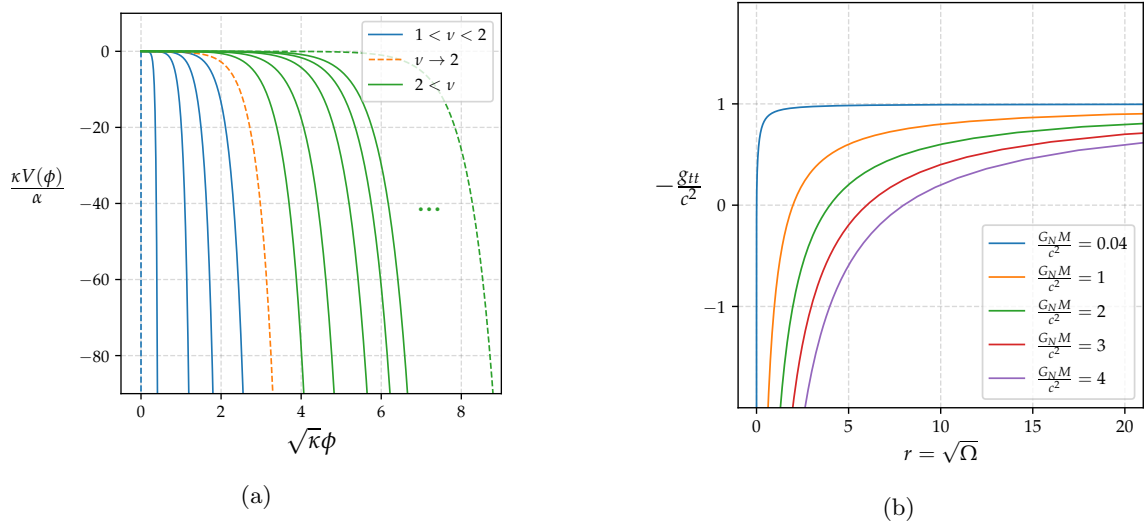


FIG. 4: Positive branch. (a): $\frac{\kappa}{\alpha}V(\phi)$ vs $\sqrt{\kappa}\phi$. (b): $-g_{tt}/c^2$ vs $\sqrt{\Omega}$, We consider the hairy parameter $\nu = 1.76$, $\alpha = -40 \text{ AU}^{-2}$ and the range of masses for the black holes $0.04 \text{ AU} \leq \frac{G_N M}{c^2} \leq 4.00 \text{ AU}$

- From figure (4b), the horizon existence, $-\frac{g_{tt}}{c^2} = 0$, is ensured if $\alpha < 0$, and for all $\nu > 1$ exist a critical minimum mass

$$M > M_{cri} \equiv \frac{c^2(\nu - 1)(\nu + 2)}{6G_N\sqrt{-\alpha(\nu + 2)}} \quad (14)$$

The existence of minimal mas giving in (13) for the negative branch ($\phi < 0$), with $\nu > 2$, can be interpreted in a similar form to Kerr-Black holes, in which the horizon existence is ensured by the inequality between the angular momentum density and mass of the black hole. In the hairy case, the horizon is ensured by the critical mass which is a function of the hairy parameters ν and α . So, if the mass M is not enough, the scalar field implodes and the horizon disappears. The positive branch has the same interpretation, but in that case the minimal mass condition is given for the entire range of values of parameter ν ($1 \leq \nu \leq \infty$), which describes the back reaction of the scalar field.

The no hair limit can be obtained if the hair parameter is fixed to $\nu = 1$. In consequence, the scalar field (4) is null and the metric (5) takes the following form

$$\Omega(x) = \frac{1}{\eta^2(x-1)^2}, \quad (15)$$

$$f(x) = \frac{1}{3}\alpha(x-1)^3 + \eta^2x(x-1)^2 \quad (16)$$

So, we can recover the Schwarzschild black hole in the canonical form by the following change of coordinates: Fixing $\nu = 1$ in (9)

$$x = 1 \pm \frac{1}{\eta r} \Rightarrow -g_{tt} = \Omega(x)f(x)|_{x(r)} = 1 - \frac{2G_N M}{c^2 r} \quad (17)$$

4 Time-like geodesics

In [34] they will show the following equations for the time-like orbits on the equatorial plane $\theta = \pi/2$, for hairy black hole solutions described in section 2. The first order orbital equation is given by³

$$\begin{aligned} \bar{\mathcal{E}}^2 - 1 &= \left(\frac{\eta\Omega(x)}{c} \right)^2 \dot{x}^2 + U_{\text{eff}}(x), \\ U_{\text{eff}}(x) &= \Omega(x)f(x) \left(1 + \frac{\bar{\mathcal{J}}^2 c^2}{\Omega(x)} \right) - 1 \end{aligned} \quad (19)$$

In order to get the second order equation we consider the following relations

$$r = \sqrt{\Omega(x)} = r(x), \quad r(\varphi) = r(x) \Rightarrow x(\varphi), \quad \varphi(\tau) \quad (20)$$

Taking the derivative of (19) with respect to φ we get a second order orbital equation which can be easily numerically solved⁴

$$\begin{aligned} \frac{d^2x}{d\varphi^2} + H(x, \bar{\mathcal{J}}, \eta) &= 0, \\ H(x, \bar{\mathcal{J}}, \eta) &= \frac{1}{2(\eta\bar{\mathcal{J}}c)^2} [(\Omega f)' + (\bar{\mathcal{J}}c)^2 f'] \end{aligned} \quad (22)$$

³Here the Killing vectors are

$$\frac{dt}{d\xi} = \frac{\bar{\mathcal{E}}}{\Omega(x)f(x)}, \quad \frac{d\varphi}{d\xi} = \frac{\bar{\mathcal{J}}c^2}{\Omega(x)}, \quad \bar{\mathcal{E}} = \mathcal{E}/mc^2, \quad \bar{\mathcal{J}} = \mathcal{J}/mc^2 \quad (18)$$

⁴It is easy to show that with the following changes we can get the orbital equation for Schwarzschild $\nu = 1$, see (A7)

$$x(\varphi) = 1 - \frac{1}{\eta r(\varphi)}, \quad \alpha = 3\eta^3 r_h - 3\eta^2, \quad r(\varphi) = \frac{1}{u(\varphi)} \quad (21)$$

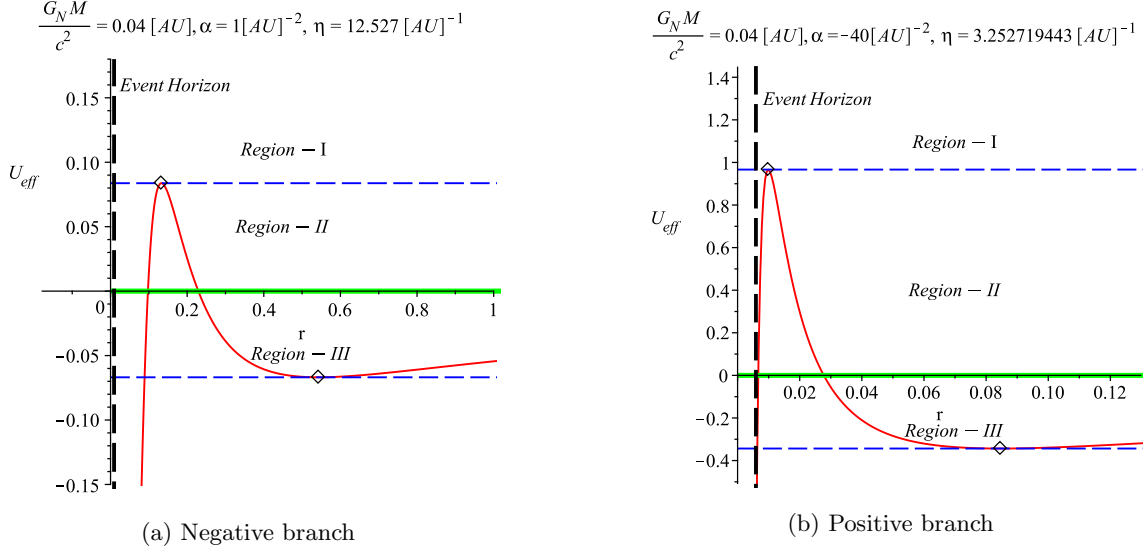


FIG. 5: We have the positive-branch (b) and negative-branch (a) of the effective potential U_{eff} . The parameters are described in table (I).

remembering that the radial coordinate is related to x -coordinate in the following exact form $r(x) = \sqrt{\frac{\nu^2 x^{\nu-1}}{\eta^2 (x^\nu - 1)^2}}$, we can plot in polar coordinates $r(x)$ vs $\varphi(x)$. The effective potential describes the following regions for negative and positive branch: Region-I: $\bar{\mathcal{E}}^2 - 1 > U(r_{max})$. Region-II: $U(r_{max}) > \bar{\mathcal{E}}^2 - 1 > 0$ and Region-III: $0 > \bar{\mathcal{E}}^2 - 1 > U_{min}$, see the Figure 5, a, b and see table (I) for the hairy parameters. Where we consider $\bar{\mathcal{E}} = \mathcal{E}/mc^2$, and $\bar{\mathcal{J}} = \mathcal{J}/mc^2$. Also in Figure 5 we can see the extremes of the effective potential U_{eff} . In this way we can set the parameters to plot a geodesic.

TABLE I: Hairy black hole and time-like geodesic parameters.

	$x < 1, \alpha = 1 AU^{-2}, \nu = 1.52$
Negative Branch	$\eta \approx 12.52655373 AU^{-1}, G_N M/c^2 = 0.04 AU$
	$\bar{\mathcal{J}} = 2.6 \times 10^{-6} yr, \bar{\mathcal{J}}_c \approx 2.1072 \times 10^{-6} yr$
	$U_{max} \approx 0.083747687, U_{min} \approx -0.0668590532$
	$x > 1, \alpha = -40 AU^{-2}, \nu = 1.76$
Positive Branch	$\eta \approx 3.252719443 AU^{-1}, G_N M/c^2 = 0.04 AU$
	$\mathcal{J} = 7 \times 10^{-7} yr, \mathcal{J}_c \approx 2.5280 \times 10^{-7} yr$
	$U_{max} \approx 0.966450101, U_{min} = -0.3435414897$

As we can see in Figure 5, apparently there is nothing new compared to the Schwarzschild case, however, in what follows we will present a new geodesic behavior given by the presence of the scalar field.

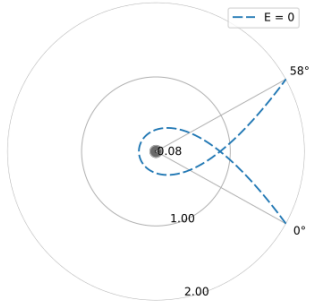
5 Hairy null geodesics

The parametric equation for null geodesics⁵ will be shown in [34], and it can be easily calculated considering $ds^2 = 0$. We replace the proper time τ by an affine parameter λ and scale it as $\lambda \rightarrow \lambda/\bar{\mathcal{J}}$

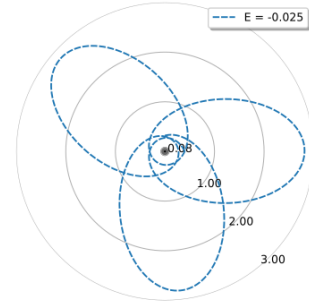
$$\eta^2 \Omega^2 \left(\frac{dx}{d\lambda} \right)^2 + \mathcal{V}(x) = \frac{c^2}{b^2}, \quad \mathcal{V}(x) = f(x)c^2 \quad (24)$$

⁵Here the Killing vectors give us

$$\frac{dt}{d\lambda} = \frac{1}{bc \Omega(x)f(x)}, \quad \frac{d\varphi}{d\lambda} = \frac{c}{\Omega(x)} \quad (23)$$

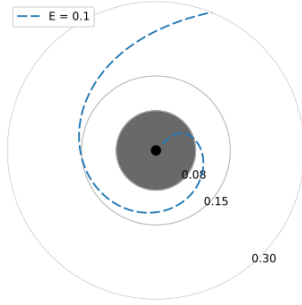


(a) $r_0 = 2 [AU]$ and $0 < \varphi < 2.5\pi$

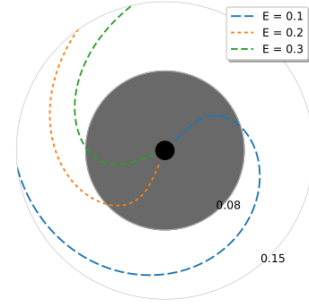


(b) $r_0 = 0.4 [AU]$ and $0 < \varphi < 8.5\pi$

FIG. 6: **Negative Branch (time-like)** In order to compare we plot the Schwarzschild black hole horizon $r_h = \frac{2G_N M}{c^2} = 0.08 AU$ (outer grey circle) and the hairy black hole horizon $\sqrt{\Omega(x_h)} = 0.009 AU$ (inner dark circle). The other constants are fixed to $\bar{J} = 2.6 \times 10^{-6} yr$, $\alpha = 1$, $\nu = 1.52$, $E = \bar{\mathcal{E}}^2 - 1$.

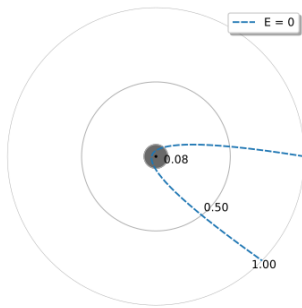


(a) $r_0 = 2 [AU]$ and $0 < \varphi < 2.5\pi$

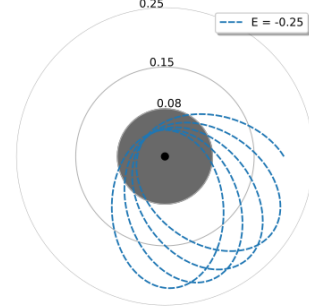


(b) $r_0 = 2 [AU]$ and $0 < \varphi < 2.5\pi$

FIG. 7: **Negative Branch (time-like)** The hairy black hole is represented by the black disk of radius $\sqrt{\Omega(x_h)} = 0.009 AU$, while the Schwarzschild black hole, by the grey disk of radius $r_h = \frac{2G_N M}{c^2} = 0.08 AU$. The constants and parameters are fixed to $\bar{J} = 2.6 \times 10^{-6} yr$, $\alpha = 1$, $\nu = 1.52$, $\eta = 12.527 AU^{-1}$, $E = \bar{\mathcal{E}}^2 - 1$.



(a) $r_0 = 1 [AU]$ and $0 < \varphi < 1.7\pi$



(b) $r_0 = 0.2 [AU]$ and $0 < \varphi < 8.5\pi$

FIG. 8: **Positive Branch (time-like)** In both figures the hairy black hole is represented by the black disk of radius $\sqrt{\Omega(x_h)} = 0.006 AU$, while the Schwarzschild black hole, by the grey disk of radius $r_h = \frac{2G_N M}{c^2} = 0.08 AU$. The constants and parameters are fixed to $\bar{J} = 7 \times 10^{-7} yr$, $\alpha = -40$, $M G_N / c^2 = 0.04$, $\nu = 1.76$, $E = \bar{\mathcal{E}}^2 - 1$.



(a) $r_0 = 0.25 [AU]$ and $0 < \varphi < 2.5\pi$

(b) $r_0 = 2 [AU]$ and $0 < \varphi < 2.5\pi$

FIG. 9: **Positive Branch (time-like)** The hairy black hole is represented by the black disk of radius $\sqrt{\Omega(x_h)} = 0.006 AU$, while the Schwarzschild black hole, by the grey disk of radius $r_h = 2G_N M / c^2 = 0.08 AU$. The other constants are fixed to $\bar{\mathcal{J}} = 7 \times 10^{-7} yr$, $\alpha = -40$, $M G_N / c^2 = 0.04$, $\nu = 1.76$, $E = \bar{\mathcal{E}}^2 - 1$.

where the effective potential $\mathcal{V}(x, \alpha, M, \nu)$ is given by

$$\mathcal{V}(x, \alpha, M, \nu) = c^2 f(x) = \alpha c^2 \left[\frac{1}{\nu^2 - 4} - \frac{x^2}{\nu^2} \left(1 + \frac{x^{-\nu}}{\nu - 2} - \frac{x^\nu}{\nu + 2} \right) \right] + \frac{x c^2}{\Omega(x, M)} \quad (25)$$

The null geodesics are completely determined by the impact parameter $b^2 \equiv (c\bar{\mathcal{J}})^2 / \bar{\mathcal{E}}^2$. In order to integrate numerically the geodesic equation we need consider the first order orbital equation for $x(\varphi)$

$$\left(\frac{dx}{d\varphi} \right)^2 = \frac{1}{\eta^2} \left[\frac{1}{b^2} - f(x) \right] \quad (26)$$

Near to boundary we can integrate (26) and using $x = 1 - 1/\eta r$ we get $r\varphi = b$, which give us the intuitive definition of the impact parameter. Taking the derivative with respect to φ in (26) we can get the second order equation

$$\frac{d^2 x}{d\varphi^2} + \frac{1}{2\eta^2} \frac{df(x)}{dx} = 0 \quad (27)$$

The extreme points of the potential where the location is x_0

$$\mathcal{V}(x_0) = \frac{c^2}{b_0^2}, \quad \frac{d\mathcal{V}(x_0)}{dx} = 0 \Rightarrow x_0' = \frac{\alpha + \eta^2(2 - \nu)}{\alpha + \eta^2(2 + \nu)} \quad (28)$$

and the radius of the minimal unstable circular orbit is $r_0 = \sqrt{\Omega(x_0)}$, whit its respective critical impact parameter b_0

$$r_0 = \pm \frac{1}{2\eta^3} [\alpha + \eta^2(2 - \nu)]^{\frac{\nu-1}{2\nu}} [\alpha + \eta^2(2 + \nu)]^{\frac{\nu+1}{2\nu}} \quad (29)$$

$x_0 < 1 (+), \quad x_0 > 1 (-)$

$$\mathcal{V}(x_0) = \frac{c^2}{b_0^2} \Rightarrow b_0 = \frac{1}{\sqrt{f(x_0)}} \quad (30)$$

Then

- The light can be deflected if $\Rightarrow \frac{c^2}{b^2} < \mathcal{V}(x_0)$
- The light get down to black hole if $\Rightarrow \frac{c^2}{b^2} > \mathcal{V}(x_0)$

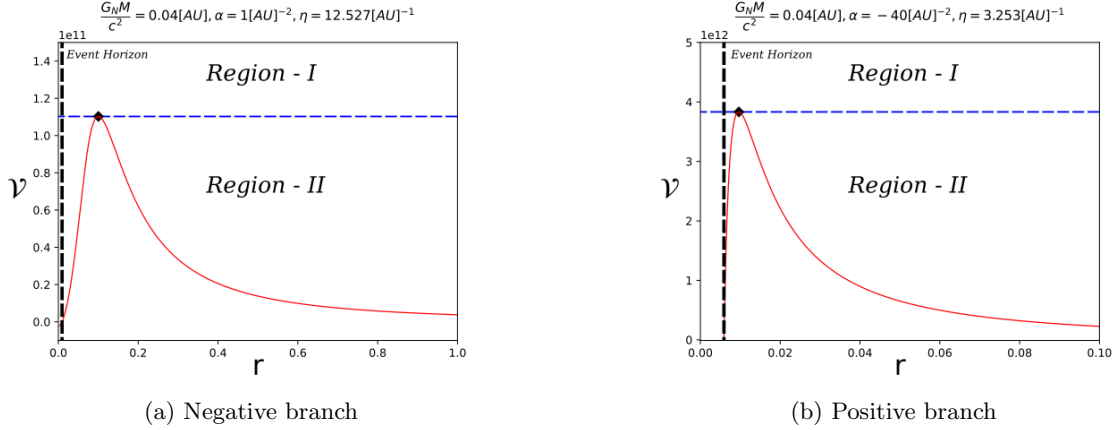


FIG. 10: We have the positive-branch (b) and negative-branch (a) of the effective potential (25). The parameters are described in table (II).

- The critical impact parameter is defined like a place in which the massless particles are trapped in an unstable circular orbit (ISCO) $\Rightarrow \mathcal{V}(x_0) = \frac{c^2}{b_0^2}$
- In the no-hair limit $\nu = 1$ the ISCO radius and the critical impact parameter are $r_0 = 3MG_N/c^2 = 0.12 AU$, $b_0 = 3\sqrt{3}MG_N/c^2 = 0.207846 AU$.

TABLE II: Hairy black hole and null geodesic parameters.

Negative Branch	$x < 1, \alpha = 1 AU^{-2}, \nu = 1.52$
	$\eta = 12.52655373 AU^{-1}, G_N M/c^2 = 0.04 AU$
	$x_0 = 0.271628, r_0 = 0.1003 AU$
	$b_0 = 0.192949 AU$
	$\mathcal{V}(x_0) = 1.07423 \times 10^{11} yr^{-2}$
Positive Branch	$x > 1, \alpha = -40 AU^{-2}, \nu = 1.76$
	$\eta = 3.252719443 AU^{-1}, G_N M/c^2 = 0.04 AU$
	$x_0 = 18.5943, r_0 = 0.0096397 AU$
	$b_0 = 0.0327298 AU$
	$\mathcal{V}(x_0) = 3.73333 \times 10^{12} yr^{-2}$

From Figure 11 we can conclude

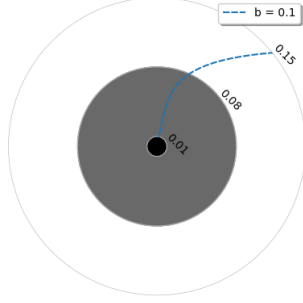
11a According to table (II) the null geodesic is defined in the region-I, see (10a), where $\frac{c^2}{b^2} = 4.10496 \cdot 10^{11} yr^{-2} > \mathcal{V}(x_0)$. A null-particle fall to the black hole, we observe that the orbit is perpendicular to the hairy black hole horizon. The backreaction in the dense hair region cause this anomalous orbit.

11b According to table (II) the null geodesic is defined in the region-II, see (10a), where $\frac{c^2}{b^2} = 0.45611 \cdot 10^{11} yr^{-2} < \mathcal{V}(x_0)$. A null-particle is deflected by the hairy black hole

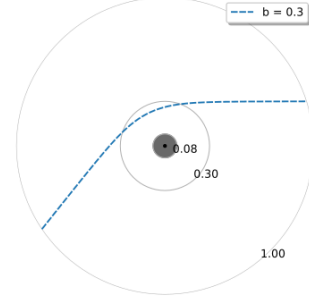
From Figure 12 we can conclude

12a According to table (II) the null geodesic is defined in region-I, see (10b), where $\frac{c^2}{b^2} = 4.56107 \cdot 10^{12} yr^{-2} > \mathcal{V}(x_0)$. A null-particle fall to the black hole, we observe that the orbit is not perpendicular to the hairy black hole horizon. That orbit is usual in Schwarzschild black hole space-time.

12b According to table (II) the null geodesic is defined in region-II, see (10b), where $\frac{c^2}{b^2} = 2.56560 \cdot 10^{12} yr^{-2} < \mathcal{V}(x_0)$. A null-particle is highly deflected. Indeed, this light deviation is impossible to find in Schwarzschild black hole space-time.

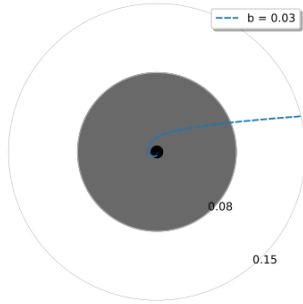


(a) $r_0 = 1$ [AU] and $0.1 < \varphi < 1.2\pi$

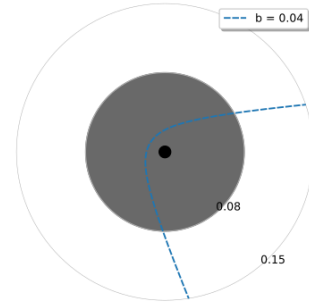


(b) $r_0 = 1$ [AU] and $0.29 < \varphi < 1.2\pi$

FIG. 11: **Negative Branch (null)**. The Schwarzschild black hole horizon is $r_h = \frac{2G_N M}{c^2}$ (grey circle) and hairy horizon $\sqrt{\Omega(x_h)}$ (black circle). The other constants are fixed to $\alpha = 1$, $M G_N / c^2 = 0.04$, $\nu = 1.52$.



(a) $r_0 = 1$ [AU] and $0.03 < \varphi < 1.7\pi$



(b) $r_0 = 1$ [AU] and $0.04 < \varphi < 1.6\pi$

FIG. 12: **Positive Branch (null)** The Schwarzschild black hole horizon is $r_h = \frac{2GM}{c^2}$ (grey disk contour) and hairy horizon $\sqrt{\Omega(x_h)}$ (black disk contour). The other constants are fixed to $\alpha = -40$, $M G_N / c^2 = 0.04$, $\nu = 1.76$.

6 Hairy near horizon geodesics

The goal of the present section is to explain the anomalous infalling time-like or space-like geodesics shown at Figure 7 and 11. In those figures the geodesics apparently go inside the black hole orthogonal to the horizon surface, here we verify that this is actually true.

Considering the solution of the hairy black hole given in section 2, the localization of the horizon x_h is such that $f(x_h) = 0$ and the near horizon geometry can be constructed under the following change $x = x_h + \epsilon$, giving us

$$\begin{aligned} f\Omega|_{x_h+\epsilon} &\approx (x - x_h)\Omega(x_h)f'(x_h), \\ \frac{f}{\Omega}|_{x_h+\epsilon} &\approx (x - x_h)\frac{f'(x_h)}{\Omega(x_h)} \end{aligned} \quad (31)$$

replacing in the hairy metric (5)

$$ds^2 = -(x - x_h)\Omega(x_h)f'(x_h)c^2 dt^2 + \frac{\eta^2 dx^2}{(x - x_h)\frac{f'(x_h)}{\Omega(x_h)}} + \Omega(x_h)(d\theta^2 + \sin^2 \theta d\varphi^2) \quad (32)$$

taking the usual transformation to radial part

$$d\rho^2 = \frac{\eta^2 dx^2}{(x - x_h)\frac{f'(x_h)}{\Omega(x_h)}} \Rightarrow \rho^2 = 4\eta^2 \frac{\Omega(x_h)}{f'(x_h)}(x - x_h) \quad (33)$$

and for the temporal coordinate $t_R = \frac{f'(x_h)}{2\eta}t$, we get the Rindler geometry

$$ds^2 = -\rho^2 dt_R^2 + d\rho^2 + \frac{\Omega(x_h)}{l^2}(d\theta^2 + \sin^2 \theta d\varphi^2) \quad (34)$$

6.1 Time-like near horizon geodesics

The near horizon geometry of (5) is described by the metric

$$\begin{aligned} ds^2 &= \Omega(x_h)\left(-F(x)c^2 dt^2 + \frac{\eta^2 dx^2}{F(x)} + d\theta^2 + \sin^2 \theta d\varphi^2\right) \\ F(x) &= (x - x_h)f'(x_h) \end{aligned} \quad (35)$$

The Killing equations give us the following conserved quantities

$$\dot{t} = \frac{\bar{\mathcal{E}}}{\Omega(x_h)F(x)}, \quad \dot{\varphi} = \frac{\bar{\mathcal{J}}c^2}{\Omega(x_h)} \quad (36)$$

And the parametric equation is

$$\begin{aligned} \bar{\mathcal{E}}^2 - 1 &= \left(\frac{\eta\Omega(x_h)}{c}\right)^2 \left(\frac{dx}{d\tau}\right)^2 + U_{\text{eff}}(x) \\ U_{\text{eff}}(x) &= \Omega(x_h)F(x)\left(1 + \frac{\bar{\mathcal{J}}^2 c^2}{\Omega(x_h)}\right) - 1 \end{aligned} \quad (37)$$

Considering the following chain-rule: $\dot{x} = \frac{dx}{d\varphi}\dot{\varphi}$, we can get the orbital equation with $E \equiv \bar{\mathcal{E}}^2 - 1$

$$E = \eta^2 \bar{\mathcal{J}}^2 c^2 \left(\frac{dx}{d\varphi}\right)^2 + U_{\text{eff}}(x) \quad (38)$$

taking the derivative with respect to φ

$$\begin{aligned} \frac{d^2x}{d\varphi^2} + H(x_h, \nu, \bar{\mathcal{J}}, \eta) &= 0, \\ H(x_h, \nu, \bar{\mathcal{J}}, \eta) &= \frac{f'(x_h)}{2(\eta\bar{\mathcal{J}}c)^2} [\Omega(x_h) + (\bar{\mathcal{J}}c)^2] \end{aligned} \quad (39)$$

the solution is

$$x(\varphi) = -\frac{H(x_h, \nu, \bar{\mathcal{J}}, \eta)}{2} \varphi^2 + c_1 \varphi + c_2 \quad (40)$$

The initial conditions are, see the example of Schwarzschild case in the B,

$$x(0) = x_h \Rightarrow c_2 = x_h, \quad \left(\frac{dx}{d\varphi} \right)_{x_h} = \frac{\bar{\mathcal{E}}}{\eta\bar{\mathcal{J}}c} = c_1 \quad (41)$$

the near-horizon solution for time-like geodesic, with (41), is

$$x(\varphi) = -\frac{H(x_h, \nu, \bar{\mathcal{J}}, \eta)}{2} \varphi^2 + \frac{\bar{\mathcal{E}}}{\eta\bar{\mathcal{J}}c} \varphi + x_h \quad (42)$$

and to plotting we consider: $r(\varphi) = \sqrt{\Omega(x(\varphi))}$

6.2 Null-like near horizon geodesics

Considering the near-horizon metric (35) and the change (36) we obtain the following expressions for conserved quantities

$$\frac{dt}{d\xi} = \frac{1}{bc \Omega(x_h) F(x)}, \quad \frac{d\varphi}{d\xi} = \frac{c}{\Omega(x_h)} \quad (43)$$

the first order orbital equation is

$$\left(\frac{dx}{d\varphi} \right)^2 = \frac{1}{\eta^2} \left[\frac{1}{b^2} - F(x) \right] \quad (44)$$

the second order and its solution is

$$\frac{d^2x}{d\varphi^2} + \frac{f'(x_h)}{2\eta^2} = 0 \Rightarrow x(\varphi) = -\frac{f'(x_h)}{4\eta^2} \varphi^2 + c_1 \varphi + c_2 \quad (45)$$

The initial conditions are

$$x(0) = x_h \Rightarrow c_2 = x_h, \quad \left(\frac{dx}{d\varphi} \right)_{x_h} = \frac{1}{\eta b} = c_1 \quad (46)$$

The near-horizon solution for time-like geodesic is, here we would like to highlight that $x(\varphi) = x(\varphi, \nu)$ depend on the hairy parameter,

$$x(\varphi) = -\frac{f'(x_h)}{4\eta^2} \varphi^2 + \frac{\varphi}{\eta b} + x_h, \quad r(\varphi) = \sqrt{\Omega(x(\varphi))} \quad (47)$$

the above solution is very similar to the Schwarzschild case (B16), however the constants that multiply φ^2 and φ depend on the hairy parameter ν , which clearly changes the usual Schwarzschild behaviour.

The Schwarzschild black hole has geodesics which fall inside of the black hole with some angle with respect to the tangent to horizon, see Figure 19, while in the hairy case we showed that geodesics cross the horizon orthogonally.

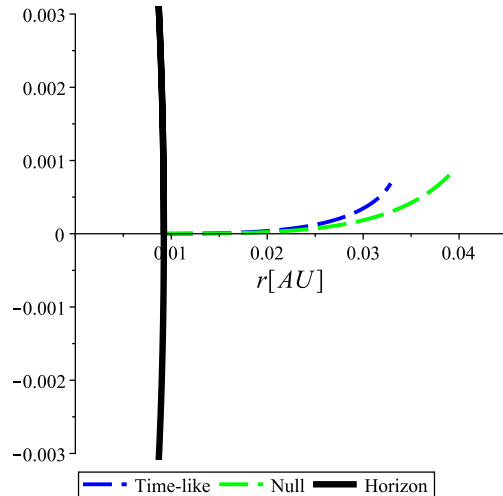


FIG. 13: **Hairy near horizon geodesics.** Here we plot the near horizon geodesics of the Figure 7b and Figure 11b, which are null and time-like respectively, using the equation (42) and (47). Here we consider the angular momenta per unit mas $\tilde{J} = 2.6 \times 10^{-6}$ and the mass of the black hole $G_N M/c^2 = 0.04$. For time-like geodesic we consider $E = 0.1$ and for null case $b = 0.1$, $E = 0.1$. The black line define the horizon of the black hole of radius $r_h = 0.0192 AU$.

7 Discussion

Our first results are the existence of the critical mass for negative branch $0 < x < 1$ with $2 < \nu$ and positive branch $1 < x < \infty$ with $\nu > 1$

$$M_{cri} \equiv \frac{c^2}{2G_N} \left(\frac{\nu - 2}{\alpha} \right)^{1/2} \quad (48)$$

$$M_{cri} \equiv \frac{c^2(\nu - 1)(\nu + 2)}{6G_N \sqrt{-\alpha(\nu + 2)}}$$

there is a black hole horizon if $M > M_{cri}$, see 3a, 3b and 4a, 4b then, the existence of the scalar field $\phi(x)$ and the non-trivial potential $V(\phi)$, forces that if there is not enough mass, the black hole could implode leaving a naked singularity. The existence of this critical mass could impose conditions on the minimal mass in modeling of the accretion disk [53, 54, 55, 56, 57]

The most important result shown in section 5 is the anomalous changing of geodesics as particles enter into the dense hair region (grey disk), see 7 and 11. Both types of geodesics go inside the hairy black hole orthogonal to the horizon surface, see 13. The great backreaction of the potential $V(\phi)$ in the dense hair region $\mathcal{D} \equiv 2MG_N/c^2 - r_h$ is the main cause of anomalous changing of geodesics trajectories. It is anomalous because, for static black hole asymptotically flat solutions, there is no similar examples in the literature. To clarify this results, in section 6 we construct the near horizon geodesics for black holes described at Figure 7 and 11, which results are shown in Figure 13. There are other hairy configurations, such as 9 and 12, that do not present the anomalous changing of geodesics. For certain values of the parameters of the theory α, ν and energy we have geodesics topologically equivalent to those of Schwarzschild black hole and for another range of parameters α, ν we obtain an anomalous behavior

The second future direction consists of studying how to take advantage of this anomalous effect in geodesics to know if it is a black hole with hair or not. A first proposal would be to launch a test satellite in a closed orbit, this will allow us to fix the parameters of the theory, α and ν , and build the effective potential similar to 5a and 5b, then we look for an energy range in region I, in which geodesics have this anomalous behavior. From a theoretical point of view we would like to find the exact range of the parameters of the theory in which this anomalous behavior exists.

In section 5 we get the radio r_0 of unstable circular orbit (ISCO), for negative branch $\phi < 0$

$$r_0 = \frac{1}{2\eta^3} [\alpha + \eta^2(2 - \nu)]^{\frac{\nu-1}{2\nu}} [\alpha + \eta^2(2 + \nu)]^{\frac{\nu+1}{2\nu}} \quad (49)$$

and, $\phi > 0$ for positive branch

$$r_0 = -\frac{1}{2\eta^3} [\alpha + \eta^2(2 - \nu)]^{\frac{\nu-1}{2\nu}} [\alpha + \eta^2(2 + \nu)]^{\frac{\nu+1}{2\nu}} \quad (50)$$

which depend on the hairy parameters α, ν and on the mass of the black hole $\eta(M, \alpha)$. Then, the shadow of the hairy black hole depend of α, ν, M . In a recent work [57], they have shown that we can constraint the hairy parameters α, ν, M based on size of the shadow of $M87^*$ black hole [32, 33]. This will be one of the topics of a future work, in addition to modeling the accretion disk

Acknowledgments

Research of WC supported by Universidad Nacional de San Antonio Abad del Cusco. The work of DC is supported by Pontificia Universidad Católica de Valparaíso. The author GV-M acknowledges the receipt of the grant from the Abdus Salam International Centre for Theoretical Physics, Trieste, Italy.

Appendix A: Schwarzschild solution

$$ds^2 = -c^2 N(r) dt^2 + \frac{dr^2}{N(r)} + r^2 (d\theta^2 + \sin^2 \theta d\varphi^2) \quad (\text{A1})$$

$$N(r) = 1 - \frac{r_h}{r} \quad (\text{A2})$$

Here, r_h is the horizon radius. The mass of the black hole is given by

$$M = \frac{c^2 r_h}{2G_N} \quad (\text{A3})$$

A.1 Time-like geodesic

Here $ds^2 = -c^2 d\tau^2$, where τ is proper time. In addition, setting the geodesic at the equatorial plane ($\theta = \pi/2$) due to the rotational isometry we obtain

$$-c^2 = -N(r)c^2 \dot{t}^2 + \frac{\dot{r}^2}{N(r)} + r^2 \dot{\varphi}^2 \quad (\text{A4})$$

The conserved quantities along the isometry orbits generated by the Killing vectors $\xi_{(t)} = \partial_t$ and $\xi_{(\varphi)} = \partial_\varphi$ are given by \mathcal{E} (dimensionless) and $\bar{\mathcal{J}}$ (yr): $dt/d\tau = \mathcal{E}/N(r)$ and $d\varphi/d\tau = \bar{\mathcal{J}}c^2/r^2$. Here $\xi_{(t)} = (c, 0, 0, 0)$ and $\xi_{(\varphi)} = (0, 0, 0, 1)$, replacing in (A4) we can get the first order orbital equation. It describes the radial motion of a test body with energy $E = \mathcal{E}^2 - 1$ in the effective potential, see Figure 14

$$E = \frac{\dot{r}^2}{c^2} + U_{\text{eff}}(r), \quad U_{\text{eff}}(r) = N(r) \left(1 + \frac{\bar{\mathcal{J}}^2 c^2}{r^2} \right) - 1 \quad (\text{A5})$$

The polar equation can be constructed considering the chain-rule $\frac{dr}{d\tau} = \frac{dr}{d\varphi} \frac{d\varphi}{d\tau}$, from that we have

$$\left(\frac{dr}{d\varphi} \right)^2 = \frac{r^4}{\bar{\mathcal{J}}^2 c^2} (E - U_{\text{eff}}), \quad \Delta\varphi = 2 \left| \int_{r_p}^{r_a} \frac{c \bar{\mathcal{J}} dr}{r^2 \sqrt{E - U_{\text{eff}}(r)}} \right| - 2\pi \quad (\text{A6})$$

the left-hand equation describe the orbit in polar coordinates, and the right-hand equation is the precession of the orbits closed for each revolution, where r_a, r_p can be solved from $\left. \frac{dr}{d\varphi} \right|_{r_a, r_p} = 0$ or $E = U_{\text{eff}}(r_a, r_p)$. The typical second order orbital equation can be get considering the following change of variables $u(\varphi) = 1/r(\varphi)$ and $du/d\varphi = -u^2 dr/d\varphi$

$$\frac{d^2 u}{d\varphi^2} + u - \frac{3r_h}{2} u^2 = \frac{1}{\lambda}, \quad \lambda = \frac{2c^2 \bar{\mathcal{J}}^2}{r_h} = \frac{2\mathcal{J}^2}{m^2 c^2 r_h} \quad (\text{A7})$$

We use the Runge-Kutta method in order to solve it

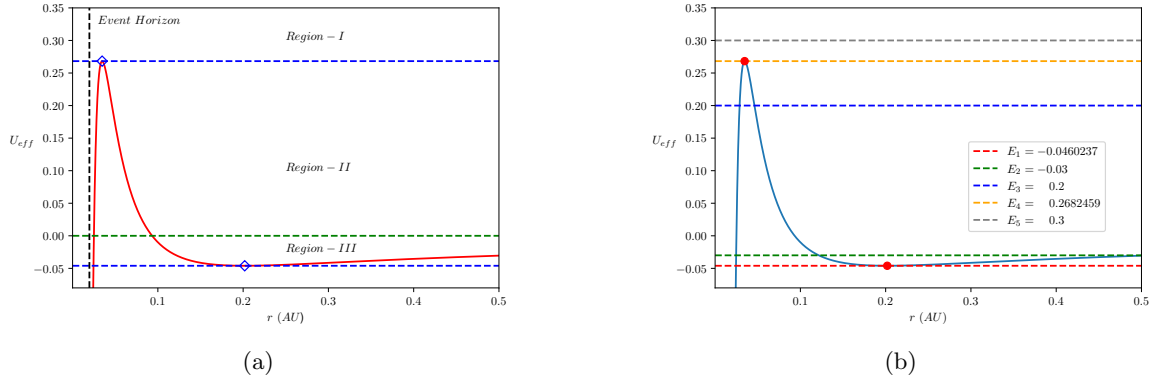
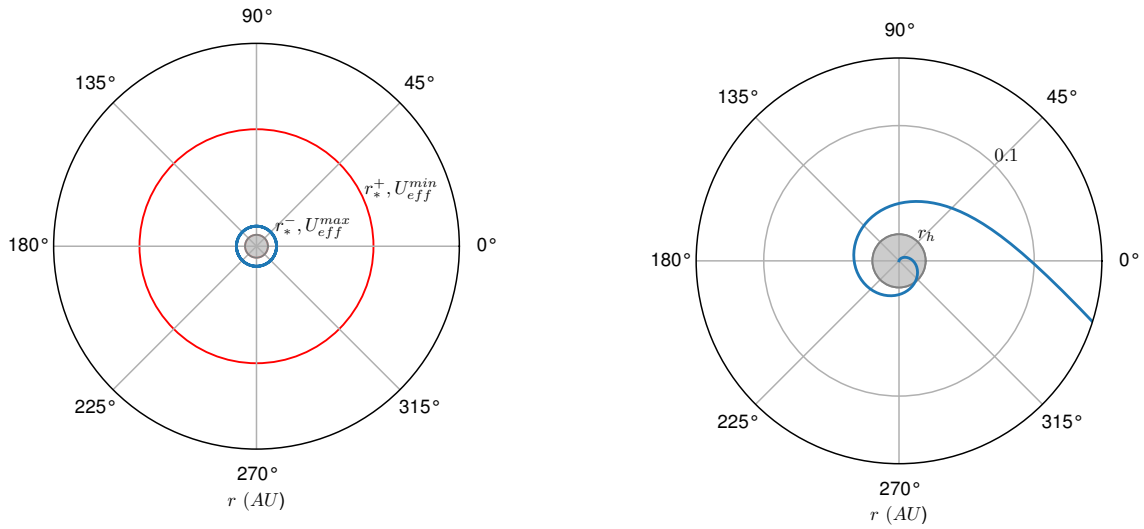


FIG. 14: (a): Region I, Above $E = U_{eff}^{max}$. Region II: Between $E = 0$ and $E = U_{eff}^{max}$. Region III: Between $E = U_{eff}^{min}$ and $E = 0$. To make this plot we have considered $\bar{\mathcal{J}}^2 = \frac{24M^2G_N^2}{c^6}$, with $M = 10^6 M_\odot$. (b): E_1 corresponds to the minimum of the effective potential. E_2 belongs to Region III. E_3 belongs to Region II. E_4 corresponds to the maximum of the effective potential. E_5 belongs to the region I.



(a) r_h , the stable circular orbit (red), and the unstable circular orbit (blue).

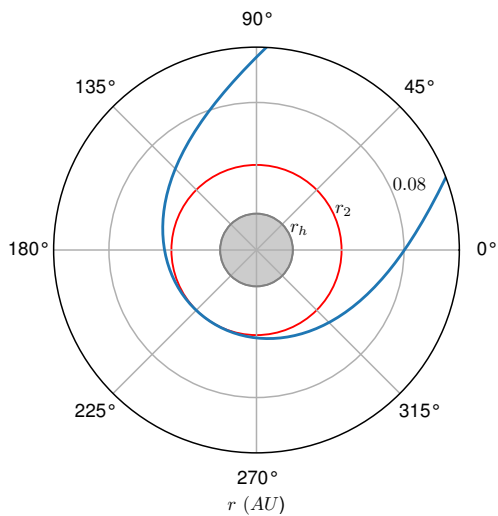
(b) r_h and the orbit (blue).

FIG. 15: **(Time-like)**

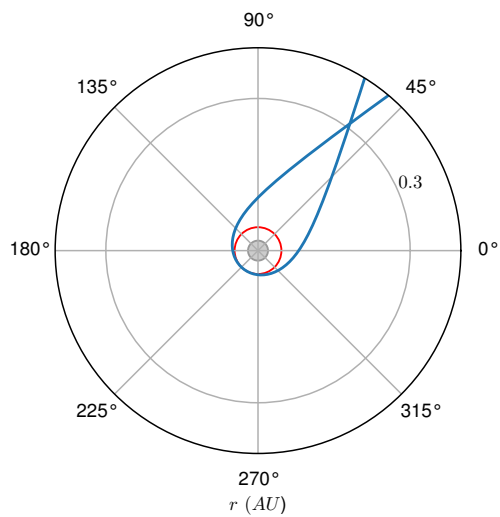
(a) $E_1 = U_{eff}^{min} = U_{eff}(r_*^+)$, initial conditions: $r_0 = r_*^+$ and $\dot{r}_0 = 0$. $E_4 = U_{eff}^{max} = U_{eff}(r_*^-)$, initial conditions: $r_0 = r_*^-$ and $\dot{r}_0 = 0$. (b) $E = E_5 = 0.3$, initial conditions: $r_0 \rightarrow \infty$ and $\dot{r}_0 = \sqrt{E}c^2$.

Orbits

Here we present the plots corresponding to each energy level presented in Figure 14.



(a) Close-up view: r_h , r_2 (red) and the orbit (blue). Where r_2 indicates the radius of the minimum distance from the center of the black hole to the orbit.



(b) Distant view: r_h , r_2 (red) and the orbit (blue)

FIG. 16: **(Time-like)**

$E = E_3 = 0.2$, initial conditions: $r_0 \rightarrow \infty$ and $\dot{r}_0 = \sqrt{E c^2}$. Where, $r_2 = 0.04613484978865398 \text{ AU}$ indicates the radius of the minimum distance from the center of the black hole to the orbit.

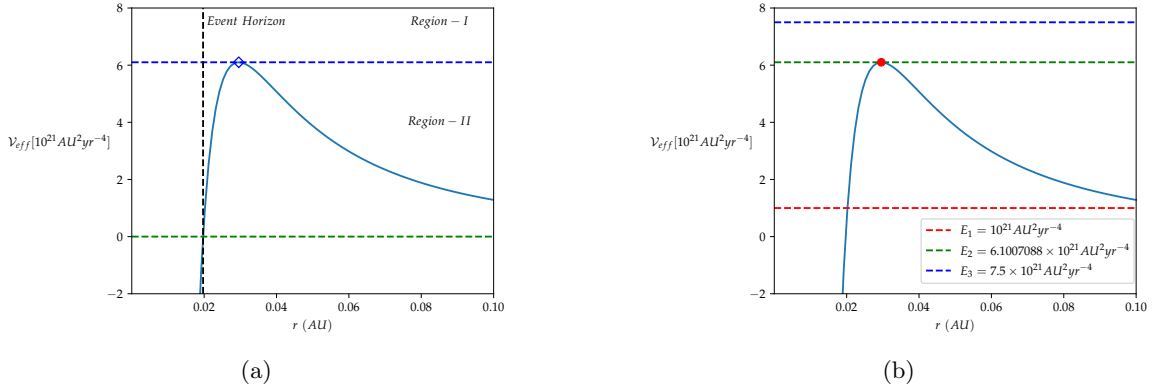


FIG. 17: (a): Region I, Above $E = \mathcal{V}_{eff}^{max}$. Region II: Between $E = 0$ and $E = \mathcal{V}_{eff}^{max}$. To make this plot we have considered $M = 10^6 M_\odot$.

(b): E_1 belongs to Region II. E_2 corresponds to the maximum of the effective potential. E_3 belongs to the region I.

A.2 Null geodesic

Here we consider an affine parameter ξ and we scale it as $\xi \rightarrow \xi/\bar{\mathcal{J}}$

$$\frac{dt}{d\xi} = \frac{\bar{\mathcal{E}}}{\bar{\mathcal{J}}N(r)}, \quad \frac{d\varphi}{d\xi} = \frac{c^2}{r^2} \quad (\text{A8})$$

replacing in (A4) at $ds^2 = 0$ we get

$$\left(\frac{dr}{d\xi}\right)^2 + \mathcal{V}_{eff}(r) = \frac{c^2}{b^2} \quad (\text{A9})$$

$$\mathcal{V}_{eff}(r) = \frac{N(r)c^4}{r^2}, \quad b^2 = \frac{\bar{\mathcal{J}}^2}{\bar{\mathcal{E}}^2}$$

considering the chain-rule $\frac{dr}{d\xi} \frac{d\xi}{d\varphi} = \frac{dr}{d\varphi}$ we have the polar equation and the deflection of a light-ray which comes from infinity, pass near to black hole R_0 and return to infinity

$$\left(\frac{dr}{d\varphi}\right)^2 = \frac{r^4}{b^2 c^2} - r^2 N, \quad \Delta\varphi = 2 \int_{R_0}^{\infty} \frac{1}{r^2} \left(\frac{1}{b^2 c^2} - \frac{N}{r^2}\right)^{-1/2} \quad (\text{A10})$$

at boundary ($r \rightarrow \infty$) that polar equation can be solved $r\varphi = bc$, from that, b is interpreted as an impact parameter. The right-hand side equation (A10) is very useful in order to get the angle of deflection of light rays coming from infinity and passing close to the black hole $r = R_0$, where R_0 comes from $\left.\frac{dr}{d\xi}\right|_{R_0} = 0$ or $\left.\frac{dr}{d\varphi}\right|_{R_0} = 0$; in the Schwarzschild case that equation is $R_0^3 - b^2 c^2 R_0 - b^2 c^2 r_h = 0$.

In the literature we usually have the following change of radial coordinate $r(\varphi) = 1/u(\varphi)$, in the left-hand side equation of (A10), in order to get the second order equation. Finally, we can transform it in two differential equations in order to apply the Runge-Kutta method to solve it.

Appendix B: Near-horizon geometry of Schwarzschild black hole

The present section is an interesting example which can help us to understand the hairy case. The near horizon geometry of Schwarzschild black hole (A1) is such that $r = r_h + \epsilon$

$$N(r) = 1 - \frac{r_h}{r} \Rightarrow N(r_h + \epsilon) \approx (r - r_h)N'(r_h) \quad (\text{B1})$$

the metric is given by

$$ds^2 = -\frac{(r - r_h)}{r_h} c^2 dt^2 + \frac{r_h dr^2}{(r - r_h)} + r_h^2 (d\theta^2 + \sin^2 \theta d\varphi^2) \quad (\text{B2})$$

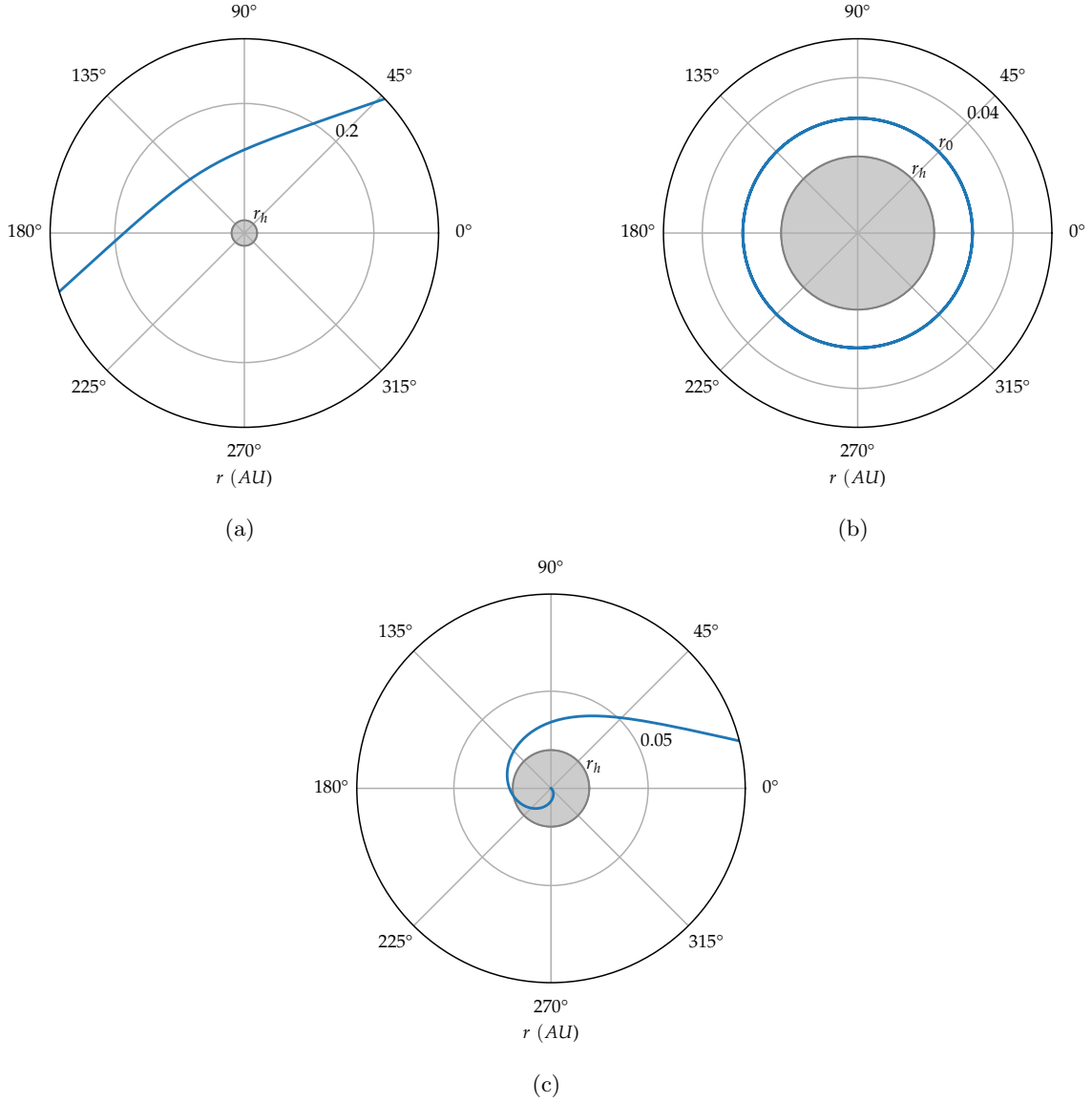


FIG. 18: (Null-like).

(a): $E = E_1 = 10^{21} AU^2 yr^{-4}$, initial conditions: $r_0 \rightarrow \infty$ and $\left(\frac{dr}{d\xi}\right)_0 = \sqrt{E}$.

(b): $E = E_2 = \mathcal{V}_{eff}^{max} = \mathcal{V}_{eff}(r_*)$, initial conditions: $r_0 = r_*$ and $\left(\frac{dr}{d\xi}\right)_0 = 0$.

(c): $E = E_1 = 7.5 \times 10^{21} AU^2 yr^{-4}$, initial conditions: $r_0 \rightarrow \infty$ and $\left(\frac{dr}{d\xi}\right)_0 = \sqrt{E}$.

The Lorentzian signature of the metric imposes the condition $r \geq r_h$. Choosing a new radial coordinate $\rho^2 = 4r_h(r - r_h)$ we get the Rindler geometry

B.1 Time-like geodesics

From (B2) the equation for time-like geodesics near to black hole is

$$-c^2 = -N(r)c^2\dot{t}^2 + \frac{\dot{r}^2}{N(r)} + r_h^2\dot{\varphi}^2, \quad N(r) = \frac{(r - r_h)}{r_h} \quad (\text{B3})$$

$$g_{tt}\xi_{(t)}^t u^t = -\frac{\mathcal{E}}{m} \quad \Rightarrow \quad \frac{dt}{d\tau} = \left(\frac{\mathcal{E}}{mc^2}\right) \frac{1}{N(r)} = \frac{r_h \bar{\mathcal{E}}}{r - r_h} \quad (\text{B4})$$

$$g_{\varphi\varphi}\xi_{(\varphi)}^\varphi u^\varphi = \frac{\mathcal{J}}{m} \quad \Rightarrow \quad \frac{d\varphi}{d\tau} = \left(\frac{\mathcal{J}}{mc^2}\right) \frac{c^2}{r_h^2} = \frac{\bar{\mathcal{J}}c^2}{r_h^2} \quad (\text{B5})$$

It describes the radial motion of a test body with energy $E = \bar{\mathcal{E}}^2 - 1$ in the effective potential

$$E = \frac{\dot{r}^2}{c^2} + U_{\text{eff}}(r), \quad U_{\text{eff}}(r) = \frac{(r - r_h)}{r_h} \left(1 + \frac{\bar{\mathcal{J}}^2 c^2}{r_h^2}\right) - 1 \quad (\text{B6})$$

The polar equation can be constructed considering the chain-rule $\frac{dr}{d\varphi} = \frac{dr}{d\tau} \frac{d\tau}{d\varphi}$, from that we have

$$\left(\frac{dr}{d\varphi}\right)^2 = \frac{r_h^4}{\bar{\mathcal{J}}^2 c^2} (E - U_{\text{eff}}) \quad (\text{B7})$$

The typical second order orbital equation can be constructed taking the the derivative (B7) with respect to φ . The orbital equation and the solution are

$$\begin{aligned} \frac{d^2 r}{d\varphi^2} &= -\frac{(\bar{\mathcal{J}}^2 c^2 + r_h^2)r_h}{2c^2 \bar{\mathcal{J}}^2} \\ \Rightarrow r(\varphi) &= -\frac{r_h}{4} \left(1 + \frac{r_h^2}{\bar{\mathcal{J}}^2 c^2}\right) \varphi^2 + c_1 \varphi + c_2 \end{aligned} \quad (\text{B8})$$

The initial condition at the horizon for $(dr/d\varphi)_{r_h}$ can be obtained from (B6), and at horizon we fix $r(\varphi)$ as

$$\left(\frac{dr}{d\varphi}\right)_{r_h} = \frac{r_h^2}{\bar{\mathcal{J}}c} \sqrt{E + 1} = c_1, \quad r(\varphi = 0) = r_h = c_2 \quad (\text{B9})$$

then, the solution (B8) under the above initial conditions is given by

$$r(\varphi) = -\frac{r_h}{4} \left(1 + \frac{r_h^2}{\bar{\mathcal{J}}^2 c^2}\right) \varphi^2 + \left(\frac{r_h^2}{\bar{\mathcal{J}}c} \sqrt{E + 1}\right) \varphi + r_h \quad (\text{B10})$$

B.2 Null geodesic

We consider an affine parameter ξ and scale it as $\xi \rightarrow \xi/\bar{\mathcal{J}}$

$$\frac{dt}{d\xi} = \frac{r_h \bar{\mathcal{E}}}{\bar{\mathcal{J}}(r - r_h)}, \quad \frac{d\varphi}{d\xi} = \frac{c^2}{r_h^2} \quad (\text{B11})$$

in (B2) at $ds^2 = 0$ we get

$$\begin{aligned} \left(\frac{dr}{d\xi}\right)^2 + \mathcal{V}_{\text{eff}}(r) &= \frac{c^2}{b^2}, \\ \mathcal{V}_{\text{eff}}(r) &= \frac{(r - r_h)c^4}{r_h^3}, \quad b^2 = \frac{\bar{\mathcal{J}}^2}{\bar{\mathcal{E}}^2} \end{aligned} \quad (\text{B12})$$

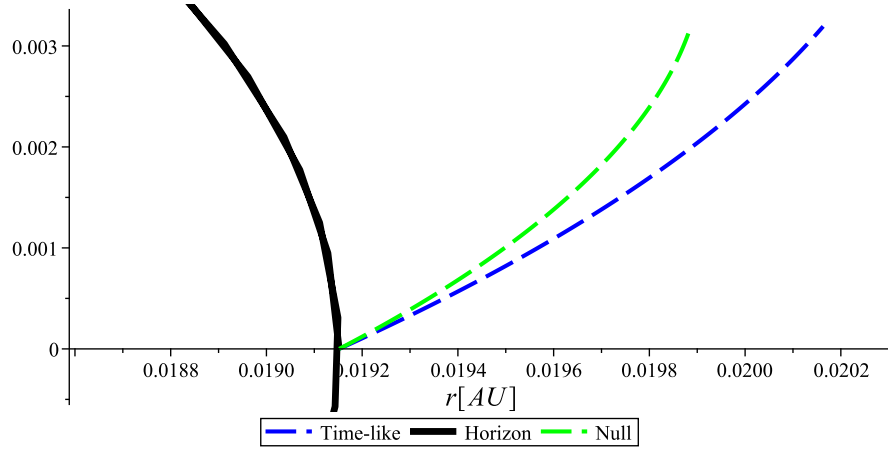


FIG. 19: **Near horizon geodesics.** Here we plot the near horizon geodesics of the figure 2b and figure 15b, which are null and time-like respectively. Here we consider the angular momentum per unit mas $\bar{\mathcal{J}} = 7.322 \times 10^{-7}$ and the mass of the black hole $M = 10^6 M_\odot$. For time-like geodesic we consider $E = 0.3$ and for null case $b^2 = 5.47329 \times 10^{-13} yr$, $E = 7.5 \times 10^{21} AU^2 yr^{-4}$. The black line define the horizon of the black hole of radius $r_h = 0.0192 AU$. The Schwarzschild black hole has a geodesics which fall inside of the black hole with some angle with respect to the tangent to horizon.

considering the chain-rule $\frac{dr}{d\xi} \frac{d\xi}{d\varphi} = \frac{dr}{d\varphi}$ we obtain the polar equation

$$\left(\frac{dr}{d\varphi}\right)^2 = \frac{r_h^4}{b^2 c^2} - r_h(r - r_h) \quad (\text{B13})$$

Taking the derivative of the orbital equation and integrating we have

$$\frac{d^2 r}{d\varphi^2} = -\frac{r_h}{2} \Rightarrow r(\varphi) = -\frac{r_h \varphi^2}{4} + c_1 \varphi + c_2 \quad (\text{B14})$$

The initial conditions are: from (B13) we get $(dr/d\varphi)_{r_h}$, and fixing that $r(\varphi = 0) = r_h$

$$\left(\frac{dr}{d\varphi}\right)_{r_h} = \frac{r_h^2}{bc} = c_1, \quad r(\varphi = 0) = r_h = c_2 \quad (\text{B15})$$

we have

$$r(\varphi) = -\frac{r_h}{2} \varphi^2 + \frac{r_h^2}{bc} \varphi + r_h \quad (\text{B16})$$

References

- [1] C. Herdeiro and E. Radu, *Phys. Rev. D* **89**, 124018 (2014), [arXiv:1406.1225 \[gr-qc\]](#) .
- [2] A. Anabalón, D. Astefanesei, A. Gallerati, and M. Trigiante, *JHEP* **04**, 058 (2018), [arXiv:1712.06971 \[hep-th\]](#) .
- [3] D. Astefanesei, C. Herdeiro, J. a. Oliveira, and E. Radu, *JHEP* **09**, 186 (2020), [arXiv:2007.04153 \[gr-qc\]](#) .
- [4] A. Anabalón, D. Astefanesei, A. Gallerati, and M. Trigiante, (2020), [arXiv:2012.09877 \[hep-th\]](#) .
- [5] M. Henneaux, C. Martinez, R. Troncoso, and J. Zanelli, *Physical Review D* **65**, 104007 (2002).
- [6] F. Correa, C. Martinez, and R. Troncoso, *Journal of High Energy Physics* **2012**, 1 (2012).
- [7] C. Martinez, R. Troncoso, and J. Zanelli, *Physical Review D* **70**, 084035 (2004).
- [8] C. Martinez and R. Troncoso, *Physical Review D* **74**, 064007 (2006).
- [9] C. Martinez, R. Troncoso, and J. Zanelli, *Physical Review D* **67**, 024008 (2003).
- [10] C. Martinez, R. Troncoso, and J. P. Staforelli, *Physical Review D* **74**, 044028 (2006).
- [11] H. C. D. L. Junior, L. C. B. Crispino, P. V. P. Cunha, and C. A. R. Herdeiro, (2021), [arXiv:2102.07034 \[gr-qc\]](#) .
- [12] N. M. Santos and C. A. R. Herdeiro, *Phys. Lett. B* **815**, 136142 (2021), [arXiv:2102.04989 \[gr-qc\]](#) .
- [13] C. A. R. Herdeiro, A. M. Pombo, E. Radu, P. V. P. Cunha, and N. Sanchis-Gual, (2021), [arXiv:2102.01703 \[gr-qc\]](#) .
- [14] D. Astefanesei, J. L. Blázquez-Salcedo, C. Herdeiro, E. Radu, and N. Sanchis-Gual, *JHEP* **07**, 063 (2020), [arXiv:1912.02192 \[gr-qc\]](#) .
- [15] A. Anabalón, D. Astefanesei, and D. Choque, *Phys. Lett. B* **743**, 154 (2015), [arXiv:1501.04252 \[hep-th\]](#) .
- [16] A. Anabalón, D. Astefanesei, and D. Choque, *Phys. Lett. B* **762**, 80 (2016), [arXiv:1606.07870 \[hep-th\]](#) .
- [17] D. Astefanesei, R. B. Mann, and R. Rojas, *JHEP* **11**, 043 (2019), [arXiv:1907.08636 \[hep-th\]](#) .
- [18] A. Anabalón, D. Astefanesei, D. Choque, and J. D. Edelstein, *JHEP* **07**, 129 (2020), [arXiv:1912.03318 \[hep-th\]](#) .
- [19] D. Astefanesei, J. Luis Blázquez-Salcedo, F. Gómez, and R. Rojas, *JHEP* **02**, 233 (2021), [arXiv:2009.01854 \[hep-th\]](#) .
- [20] D. Astefanesei, D. Choque, F. Gómez, and R. Rojas, *JHEP* **03**, 205 (2019), [arXiv:1901.01269 \[hep-th\]](#) .
- [21] A. Aceña, A. Anabalón, D. Astefanesei, and R. Mann, *JHEP* **01**, 153 (2014), [arXiv:1311.6065 \[hep-th\]](#) .
- [22] A. Anabalón, D. Astefanesei, and R. Mann, *JHEP* **10**, 184 (2013), [arXiv:1308.1693 \[hep-th\]](#) .
- [23] A. Anabalón and N. Deruelle, *Phys. Rev. D* **88**, 064011 (2013), [arXiv:1307.2194 \[gr-qc\]](#) .
- [24] A. Anabalón and D. Astefanesei, *Phys. Lett. B* **727**, 568 (2013), [arXiv:1309.5863 \[hep-th\]](#) .
- [25] A. Anabalón and D. Astefanesei, *Phys. Lett. B* **732**, 137 (2014), [arXiv:1311.7459 \[hep-th\]](#) .
- [26] A. Anabalón, D. Astefanesei, D. Choque, A. Gallerati, and M. Trigiante, (2020), [arXiv:2012.01289 \[hep-th\]](#) .
- [27] T. Hertog, *Phys. Rev. D* **74**, 084008 (2006), [arXiv:gr-qc/0608075](#) .
- [28] D. Astefanesei, H. Nastase, H. Yavartanoo, and S. Yun, *JHEP* **04**, 074 (2008), [arXiv:0711.0036 \[hep-th\]](#) .

- [29] C. Herdeiro, E. Radu, and H. Rúnarsson, *Class. Quant. Grav.* **33**, 154001 (2016), [arXiv:1603.02687 \[gr-qc\]](#) .
- [30] F. H. Vincent, E. Gourgoulhon, C. Herdeiro, and E. Radu, *Phys. Rev. D* **94**, 084045 (2016), [arXiv:1606.04246 \[gr-qc\]](#) .
- [31] D. Nunez, H. Quevedo, and D. Sudarsky, *Phys. Rev. Lett.* **76**, 571 (1996), [arXiv:gr-qc/9601020](#) .
- [32] E. H. T. Collaboration *et al.*, arXiv preprint [arXiv:1906.11238](#) (2019).
- [33] K. Akiyama, A. Alberdi, W. Alef, K. Asada, R. Azulay, A.-K. Bacsko, D. Ball, M. Baloković, J. Barrett, D. Bintley, *et al.*, *The Astrophysical Journal Letters* **875**, L6 (2019).
- [34] D. Choque, W. Dael, and R. Rojas, [xxxxxx, xxxx:To appear](#) .
- [35] G. Van Rossum and F. L. Drake, *Python 3 Reference Manual* (CreateSpace, Scotts Valley, CA, 2009).
- [36] C. R. Harris, K. J. Millman, S. J. van der Walt, R. Gommers, P. Virtanen, D. Cournapeau, E. Wieser, J. Taylor, S. Berg, N. J. Smith, R. Kern, M. Picus, S. Hoyer, M. H. van Kerkwijk, M. Brett, A. Haldane, J. F. del Río, M. Wiebe, P. Peterson, P. Gérard-Marchant, K. Sheppard, T. Reddy, W. Weckesser, H. Abbasi, C. Gohlke, and T. E. Oliphant, *Nature* **585**, 357 (2020).
- [37] P. Virtanen, R. Gommers, T. E. Oliphant, M. Haberland, T. Reddy, D. Cournapeau, E. Burovski, P. Peterson, W. Weckesser, J. Bright, S. J. van der Walt, M. Brett, J. Wilson, K. J. Millman, N. Mayorov, A. R. J. Nelson, E. Jones, R. Kern, E. Larson, C. J. Carey, Í. Polat, Y. Feng, E. W. Moore, J. VanderPlas, D. Laxalde, J. Perktold, R. Cimrman, I. Henriksen, E. A. Quintero, C. R. Harris, A. M. Archibald, A. H. Ribeiro, F. Pedregosa, P. van Mulbregt, and SciPy 1.0 Contributors, *Nature Methods* **17**, 261 (2020).
- [38] J. D. Hunter, *Computing in Science & Engineering* **9**, 90 (2007).
- [39] W. Ccuiro, “hairyBH,” <https://pypi.org/project/hairyBH/> (2021).
- [40] G. Valdivia-Mera, “Orbits-in-Schwarzschild-spacetime,” <https://github.com/gcvaldivia/Orbits-in-Schwarzschild-spacetime> (2021).
- [41] A. Anabalón, B. de Wit, and J. Oliva, *JHEP* **09**, 109 (2020), [arXiv:2001.00606 \[hep-th\]](#) .
- [42] A. Anabalón and J. Oliva, *Phys. Rev. D* **86**, 107501 (2012), [arXiv:1205.6012 \[gr-qc\]](#) .
- [43] A. Acena, A. Anabalón, and D. Astefanesei, *Phys. Rev. D* **87**, 124033 (2013), [arXiv:1211.6126 \[hep-th\]](#) .
- [44] A. Anabalón, D. Astefanesei, D. Choque, and C. Martínez, *JHEP* **03**, 117 (2016), [arXiv:1511.08759 \[hep-th\]](#) .
- [45] D. Astefanesei and E. Radu, *Phys. Rev. D* **73**, 044014 (2006), [arXiv:hep-th/0509144](#) .
- [46] D. Astefanesei, R. B. Mann, M. J. Rodríguez, and C. Stelea, *Class. Quant. Grav.* **27**, 165004 (2010), [arXiv:0909.3852 \[hep-th\]](#) .
- [47] D. Astefanesei, R. B. Mann, and C. Stelea, *Phys. Rev. D* **75**, 024007 (2007), [arXiv:hep-th/0608037](#) .
- [48] D. Astefanesei, M. J. Rodríguez, and S. Theisen, *JHEP* **08**, 046 (2010), [arXiv:1003.2421 \[hep-th\]](#) .
- [49] A. Anabalón, D. Astefanesei, and C. Martínez, *Phys. Rev. D* **91**, 041501 (2015), [arXiv:1407.3296 \[hep-th\]](#) .
- [50] K. Skenderis, *Class. Quant. Grav.* **19**, 5849 (2002), [arXiv:hep-th/0209067](#) .
- [51] S. de Haro, S. N. Solodukhin, and K. Skenderis, *Commun. Math. Phys.* **217**, 595 (2001), [arXiv:hep-th/0002230](#) .
- [52] P. Kraus, F. Larsen, and R. Siebelink, *Nucl. Phys. B* **563**, 259 (1999), [arXiv:hep-th/9906127](#) .

- [53] P. V. P. Cunha, N. A. Eiró, C. A. R. Herdeiro, and J. P. S. Lemos, *JCAP* **03**, 035 (2020), [arXiv:1912.08833 \[gr-qc\]](#) .
- [54] S. X. Tian and Z.-H. Zhu, *Phys. Rev. D* **100**, 064011 (2019), [arXiv:1908.11794 \[gr-qc\]](#) .
- [55] O. Porth, H. Olivares, Y. Mizuno, Z. Younsi, L. Rezzolla, M. Moscibrodzka, H. Falcke, and M. Kramer, (2016), [10.1186/s40668-017-0020-2](#), [arXiv:1611.09720 \[gr-qc\]](#) .
- [56] P. V. P. Cunha and C. A. R. Herdeiro, *Gen. Rel. Grav.* **50**, 42 (2018), [arXiv:1801.00860 \[gr-qc\]](#) .
- [57] P. Kocherlakota, L. Rezzolla, H. Falcke, C. M. Fromm, M. Kramer, Y. Mizuno, A. Nathanail, H. Olivares, Z. Younsi, K. Akiyama, A. Alberdi, W. Alef, J. C. Algaba, R. Anantua, K. Asada, R. Azulay, A.-K. Baczko, D. Ball, M. Baloković, J. Barrett, B. A. Benson, D. Bintley, L. Blackburn, R. Blundell, W. Boland, K. L. Bouman, G. C. Bower, H. Boyce, M. Bremer, C. D. Brinkerink, R. Brissenden, S. Britzen, A. E. Broderick, D. Brogiere, T. Bronzwaer, D.-Y. Byun, J. E. Carlstrom, A. Chael, C.-k. Chan, S. Chatterjee, K. Chatterjee, M.-T. Chen, Y. Chen, P. M. Chesler, I. Cho, P. Christian, J. E. Conway, J. M. Cordes, T. M. Crawford, G. B. Crew, A. Cruz-Osorio, Y. Cui, J. Davelaar, M. De Laurentis, R. Deane, J. Dempsey, G. Desvignes, S. S. Doeleman, R. P. Eatough, J. Farah, V. L. Fish, E. Fomalont, R. Fraga-Encinas, P. Friberg, H. A. Ford, A. Fuentes, P. Galison, C. F. Gammie, R. García, O. Gentaz, B. Georgiev, C. Goddi, R. Gold, J. L. Gómez, A. I. Gómez-Ruiz, M. Gu, M. Gurwell, K. Hada, D. Haggard, M. H. Hecht, R. Hesper, L. C. Ho, P. Ho, M. Honma, C.-W. L. Huang, L. Huang, D. H. Hughes, S. Ikeda, M. Inoue, S. Issaoun, D. J. James, B. T. Jannuzi, M. Janssen, B. Jeter, W. Jiang, A. Jimenez-Rosales, M. D. Johnson, S. Jorstad, T. Jung, M. Karami, R. Karuppusamy, T. Kawashima, G. K. Keating, M. Kettenis, D.-J. Kim, J.-Y. Kim, J. Kim, J. Kim, M. Kino, J. Y. Koay, Y. Kofuji, P. M. Koch, S. Koyama, C. Kramer, T. P. Krichbaum, C.-Y. Kuo, T. R. Lauer, S.-S. Lee, A. Levis, Y.-R. Li, Z. Li, M. Lindqvist, R. Lico, G. Lindahl, J. Liu, K. Liu, E. Liuzzo, W.-P. Lo, A. P. Lobanov, L. Loinard, C. Lonsdale, R.-S. Lu, N. R. MacDonald, J. Mao, N. Marchili, S. Markoff, D. P. Marrone, A. P. Marscher, I. Martí-Vidal, S. Matsushita, L. D. Matthews, L. Medeiros, K. M. Menten, I. Mizuno, J. M. Moran, K. Moriyama, M. Moscibrodzka, C. Müller, G. Musoke, A. M. Mejías, H. Nagai, N. M. Nagar, M. Nakamura, R. Narayan, G. Narayanan, I. Natarajan, J. Neilsen, R. Neri, C. Ni, A. Noutsos, M. A. Nowak, H. Okino, G. N. Ortiz-León, T. Oyama, F. Özel, D. C. M. Palumbo, J. Park, N. Patel, U.-L. Pen, D. W. Pesce, V. Piétu, R. Plambeck, A. PopStefanija, O. Porth, F. M. Pörtl, B. Prather, J. A. Preciado-López, D. Psaltis, H.-Y. Pu, V. Ramakrishnan, R. Rao, M. G. Rawlings, A. W. Raymond, A. Ricarte, B. Ripperda, F. Roelofs, A. Rogers, E. Ros, M. Rose, A. Roshanineshat, H. Rottmann, A. L. Roy, C. Ruzszyk, K. L. J. Rygl, S. Sánchez, D. Sánchez-Arguelles, M. Sasada, T. Savolainen, F. P. Schloerb, K.-F. Schuster, L. Shao, Z. Shen, D. Small, B. W. Sohn, J. SooHoo, H. Sun, F. Tazaki, A. J. Tetarenko, P. Tiede, R. P. J. Tilanus, M. Titus, K. Toma, P. Torne, T. Trent, E. Traianou, S. Trippe, I. van Bemmell, H. J. van Langevelde, D. R. van Rossum, J. Wagner, D. Ward-Thompson, J. Wardle, J. Weintroub, N. Wex, R. Wharton, M. Wielgus, G. N. Wong, Q. Wu, D. Yoon, A. Young, K. Young, F. Yuan, Y.-F. Yuan, J. A. Zensus, G.-Y. Zhao, and S.-S. Zhao (EHT Collaboration), *Phys. Rev. D* **103**, 104047 (2021).